SI Appendix

Spitschan et al., *The human visual cortex response to melanopsin-directed stimulation is accompanied by a distinct perceptual experience*

SI Text: Online Methods

Pre-registration. The experiments were the subject of pre-registration documents. Data collection followed the pre-registration documents in regard to the number of subjects, extent of data collection, stimulus generation, and exclusion criteria. In some cases addenda were submitted to the pre-registration before data collection began, with the pre-registered protocol being that which includes the modifications specified in these pre-data-collection addenda. In some cases the analysis approach presented in this paper differs from that described in the pre-registered protocol. Table S3 lists all pre-registration documents by experiment and deviations from the registered protocols. Some deviations were detailed in addenda submitted after data collection began, and these are also included as deviations in the table.

Subjects and subject preparation. Four subjects participated in the fMRI and pupillometry studies. All four participants are scientific investigators and three are authors of this study (4 males, ages 27, 28, 32, 46 years). These four participants choose to identify themselves by their initials. An additional 20 subjects participated in the perception experiment (9 men, 11 women, mean age 27, range 20-33); their data have been assigned anonymous study identification labels. All subjects were screened for normal color vision (1) and corrected acuity of 20/40 or better as assessed by the Snellen chart at a 20 ft distance. All subjects were studied at the University of Pennsylvania. The research was approved by the University of Pennsylvania Institutional Review Board and conducted in accordance with the principles of the Declaration of Helsinki. All subjects gave informed written consent.

Prior to fMRI scanning or perceptual rating, each subject underwent pharmacological dilation of the right eye (1% tropicamide ophthalmic with 0.5% proparacaine as a local anesthetic agent).

Visual stimuli. We used the method of silent substitution with a digital light synthesis engine (OneLight Spectra) to stimulate targeted photoreceptors. Our device produces stimulus spectra as mixtures of 56 independent, ~16 nm FWHM primaries under digital control, and can modulate between these spectra at 256 Hz. Details regarding the device, stimulus generation, and estimates of precision have been previously reported (2–4).

Our estimates of photoreceptor spectral sensitivities were as previously described (3), following the CIE physiological cone fundamentals (5). They account for the size of the visual field (64°), subject age, and the pupil size, which we assumed to be 8 mm in diameter under pharmacologic dilation.

Separate background and modulation spectra were identified to maximize available contrast on melanopsin and the combined stimulation of the L, M, and S cones. First, "mid-background" settings were selected so as to maximize available melanopsin (or LMS) Michelson contrast for modulations symmetric around this background. Then, a 66.66% modulation was found. The negative "arm" of this modulation served as the experimental background, and the positive "arm" of this modulation represented the maximal, 400% contrast pulse (Figures 1 in the main article and Figure S1). The background for the LMS, Mel, and Splatter modulations were all nominally rod-saturating (100–200 cd/m^2; >3.3 $\log_{10}$ sc td). The modulations did not explicitly silence penumbral cones (3).

We elected not to perform psychophysical nulling of our stimuli for two reasons. First, in an earlier study (2) we found that the test-retest reliability of nulling values produced by individual observers was not high. We estimated that stimulus adjustment for individual subjects was more likely to worsen photoreceptor silencing than to improve it. Second, we found that allowing for stimulus adjustment would reduce the available gamut in our modulations, with the consequence of a substantial reduction in available contrast on melanopsin.

We measured the melanopsin 400% background and stimulation spectra for a reference observer (32 years) before and after each scanning session for each subject during our initial fMRI experiment (described as Experiment 1 below). We calculated the average postreceptoral contrast for each of these 8 spectra (4 subjects × 2 measurements) with respect to the cone fundamentals assumed for the reference observer. From these measurements, we derived 8 sets of postreceptoral contrast values for LMS, L–M, and S–[L+M]. We then took the sign preserved absolute maximum value across each of the sets of 8 measurements. The resulting postreceptoral contrast values [%] were LMS: +2.173; L–M: +0.877; S–[L+M]: −10.451. Converted to cone contrast values [%] these were L: +3.050; M: +1.296; S: −8.278. We term this set of cone contrasts the 1x splatter control modulation. When presented to individual observers, the splatter control modulation was tailored to the age of the individual observers, such that even though the spectra seen by the observers would be different, they would all see a modulation with the nominal contrast values above, calculated using their age-corrected cone fundamentals.

The stimulus was viewed within an MRI compatible eye piece that provided a circular, uniform field of 64° diameter. The central 5° diameter was obscured. Subjects were asked to maintain fixation in the center of this obscured region to avoid stimulation within the macula, where spatial variation in macular pigment could alter the spectral properties of the stimulus.

Three-second pulses of spectral change were presented during individual trials of 16 s duration. During each trial, a transition from the background to the stimulation spectrum would occur starting at either 0, 1, or 2 seconds after trial onset (randomized uniformly across trials); this jitter was designed to reduce the ability of the subject to anticipate the moment of stimulus onset and to render trial timing asynchronous with respect to BOLD fMRI image acquisition. The transition from the background to the modulation spectrum, and the return to background, was subjected to a 500 ms half-cosine window.

The half-cosine windowing of the stimulus was designed to minimize perception of a Purkinje tree percept in our uniform spatial stimuli (3). Consider that there are both penumbral cones (that receive the stimulus spectrum after filtering through retinal blood vessels) and open-field cones, that receive the un-filtered stimulus. We have found previously that we can induce a percept of the retinal blood vessels using a uniform-field stimulus when two conditions are met: First, there is spatial contrast between the penumbral and open-field cones, and second, this spatial contrast is modulated at 4 Hz and higher (3). Both the LMS and melanopsin-directed spectral stimuli produce differential spatial contrast on the penumbral and open-field cones, satisfying the first condition. Critically, however, the Purkinje tree percept is reduced for these stimuli when modulated at 4 Hz and below. We windowed our stimuli with a 500 ms half-cosine at onset and offset. This corresponds to a 1 Hz modulation, and is thus comfortably below the slew rate that we have observed is needed to produce a spatial Purkinje tree percept.

Simulation of biological variability causing inadvertent cone contrast. To address the amount of inadvertent stimulation of the L, M and S cones due to biological variability not captured by the CIE model for the cone

fundamentals (Figure S5), we performed simulations of colorimetric observers, assuming variability in the following eight parameters: lens density, macular pigment density; L cone photopigment density, M cone photopigment density, S cone photopigment density; and the peak absorbance λ_{max} of the L, M and S cone photopigments. Using previously published estimates of the standard deviations in those parameters (6), we randomly sampled independently from normal distributions with those SDs. The SDs were ±18.7% deviation in lens density, ±25% in macular pigment density; ±9% deviation in L cone density, ±9% deviation in M cone density, ±7.4% deviation in S cone density; and ±2 nm, ±1.5 nm and ±1.3 nm in λ_{max} for L, M and S cones respectively. Note that the variation in lens density was taken around the age-appropriate mean density for each subject. We performed this resampling 1,000 times, generating 1,000 sets of spectral sensitivities. This was done for the four observers from the fMRI studies (Figure S5) and the twenty observers from the perceptual studies (Figure S11).

We present plots of the L, M, and S cone contrasts after transformation to a postreceptoral opponent representation assuming mechanism sensitivities to cone contrast for luminance, red-green, and blue-yellow mechanisms of [0.5 0.5 0], [0.5 −0.5 0], and [−0.5 −0.5 1] respectively. This transformation corresponds to the DKL opponent color space representation (7) when the background produces equal excitations in the L, M and S cones, for the case in which the L and M cone spectral sensitivities are scaled so that they sum to produce the luminous efficiency curve. We regarded this as a reasonable choice of reference conditions to define the transformation, as it leads to intuitively straightforward properties of the assumed postreceptoral mechanisms. We note that for other backgrounds, this transformation will describe the opponent mechanism responses to the extent that those responses are the same for modulations seen against different backgrounds, when the LMS cone contrasts of the modulations are matched across backgrounds.

Design of MRI experiments. Each of the four primary subjects participated in six MRI experiments (except for subject ASO who was unavailable to participate in the final, sixth experiment). The first two experiments presented pulses of either 400% melanopsin contrast only (Experiment 1) or 400% LMS contrast only (Experiment 2). Three experiments presented intermixed trials of different intensity of either "splatter" cone contrast (Experiment 3), melanopsin contrast (Experiment 4), or LMS contrast (Experiment 5). The final experiment (described in Figure S6) presented blocks of flickering L–M and melanopsin / rod modulations under scotopic and photopic conditions. During Experiments 1, 2, 3, and 6, the left eye was covered with an opaque patch. During Experiments 4 and 5 the left eye was uncovered and monitored with an infrared video camera (described below).

Each experimental session was approximately two hours. A given scanning session examined a single stimulus type (e. g., LMS, melanopsin, or splatter). The subject maintained adaptation to the background spectrum between trials and scan runs. Prior to each fMRI session, subjects underwent monocular dark adaptation for 20 minutes by wearing swimming goggles with the right eye obscured. Once in the scanner, the right eye was adapted for at least five minutes to the stimulus background prior to the start of functional scanning.

Experiments 3, 4 and 5 sought to measure the contrast response function (CRF) that related stimulus contrast to BOLD fMRI response. A set of stimuli of varying contrasts were presented in an intermixed order during a given scan. The LMS and melanopsin CRF studies presented five logarithmically spaced contrast levels (25, 50, 100, 200, and 400% contrast); the splatter CRF study presented 4 levels ($\frac{1}{4}\times$, $\frac{1}{2}\times$, 1×, 2×). The 2× stimulus was in fact 1.95× due to limitations in device gamut; we adopt the technically inaccurate label for ease of description and interpretation. Ordering of these trial types within and across scans followed a pseudo-random, counter-balanced order (8).

Functional MRI data collection took place during individual scans of 336 s duration. Between 9 and 12 scan runs were collected for each subject for each experiment. With the exception of Experiment 6, each scan run presented 21, 16 s trials; Experiment 6 presented blocks of stimulation and is described in Figure S6. Eighteen of the trials presented a spectral pulse. Three randomly selected trials presented an "attention event" instead of a stimulus pulse, during which the stimulus field dimmed for 500 ms. The subject was asked to press a button on a response pad when these dimming events occurred. Subjects performed well on this detection task. Collapsing performance across subjects and experiments, there were 0 false alarm responses during the 3,816 stimulus trials, and 11 misses during the 636 attention trials.

MRI data acquisition and initial processing. MRI scanning parameters made use of the Human Connectome Project LifeSpan protocol (VD13D) implemented on a 3-Tesla Siemens Prisma with a 64-channel Siemens head coil. A T1-weighted, 3D, magnetization-prepared rapid gradient-echo (MPRAGE) image was acquired for each subject in axial orientation with 0.8 mm isotropic voxels, repetition time (TR) = 2.4 s, echo time (TE) = 2.22 ms, inversion time (TI) = 1000 ms, field of view (FoV) = 256 mm, flip angle = 8°. BOLD fMRI data were obtained over 72 axial slices with 2 mm isotropic voxels with multi-band = 8, TR = 800 ms, TE = 37 ms, FOV = 208 mm, flip angle = 52°. Head motion was minimized with foam padding. Although continuous pulse-oximetry was recorded, this physiologic measurement was not used in the fMRI data analysis.

The FreeSurfer (v5.3) toolkit (`http://surfer.nmr.mgh.harvard.edu/`) (9–12) was used to process anatomical MPRAGE images to construct inflated brain surfaces and register data from across subjects for surface visualization. Briefly, this processing includes spatial inhomogeneity correction, non-linear noise-reduction, skull-stripping (13), subcortical segmentation (14, 15), intensity normalization (16), surface generation (9, 10, 17), topology correction (18, 19), surface inflation (10), and registration to a spherical atlas (11).

Raw echo-planar volumetric data were motion corrected using the FMRIB Software Library (FSL) toolkit (`http://fsl.fmrib.ox.ac.uk/fsl/`). Motion corrected functional volumes were co-registered to subject-specific anatomy in Freesurfer using FSL-FLIRT with 6 degrees-of-freedom under a FreeSurfer wrapper (`bbregister`).

BOLD fMRI time-series analysis. The pipeline for the analysis of the BOLD fMRI time series is available on GitHub (`https://github.com/gkaguirrelab/MRklar/releases/tag/v1.0.0`). Noise regressors were derived from the left, right, third, and fourth ventricles, as well as white matter, brain stem white matter, and non-brain tissue. Binary masks of these regions were initially identified in a Freesurfer anatomical segmentation volume (`aseg.mgz`). After co-registering to the functional volume, these regions were eroded by two voxels (for the white matter mask) or a single voxel (for all other regions) to avoid partial volume contamination from gray matter. The first five principal components of the time-series data across all voxels in these regions were then used as regressors. The signal from white matter local to each voxel was obtained and regressed. To obtain the local white matter signal for each voxel, the mean time series of all white matter voxels within a 15 mm radius sphere was regressed from the time series of the voxel found at the center of the sphere. This local white matter procedure was modeled after the ANATICOR pipeline

in AFNI (20). Twenty-four motion regressors were derived from the initial six parameters that result from motion correction (21). The effects of these nuisance covariates were removed from the time-series data by regression. Finally, the time-series was subjected to a high-pass Butterworth filter with a cut-off of 0.01 Hz.

The primary analyses of the study were conducted within a V1 region of interest. A cortical surface atlas (22) was used to define a patch of V1 cortex corresponding to the radial eccentricity range of 5–25°. For each subject, the average, post-processed signal within this region (and across the two hemispheres) was obtained for each scan run in each experiment. The regional time-series data were analyzed within a non-linear temporal fitting engine (`https://github.com/gkaguirrelab/temporalFittingEngine`).

As the timing of stimulus events (both spectral pulses and attention events) were asynchronous with respect to image acquisition (TRs), we derived the average evoked BOLD fMRI response for each stimulus type using a Fourier basis set approach (23). This approach provided an accurate estimate of the underlying response not available from a simple averaging of the time-series data itself across trials. The 16 s following the onset of each event was modeled with 8 harmonic pairs (a sine and cosine), ranging in frequency from 0.0625 to 1 Hz. The fit of the Fourier basis set to the evoked response was then averaged across scan runs. Because of jitter introduced into the timing of onset of each event, the inter-stimulus-interval (ISI) ranged between 14 and 18 seconds. Because the stimulus order was counterbalanced, the additive effects of trial overlap (for when the ISI was <16 seconds) should be estimated efficiently and without bias by the model. Any non-linear interactions caused by hemodynamic response overlap will not be captured in our model, but we are reassured that there is nothing unusual in the appearance of the evoked response estimates between 14 and 16 seconds.

The evoked responses obtained in this way to the spectral pulse stimuli are presented in Figures 2d, 2e and S2. As the attention events were brief (500 ms), the average evoked response to the attention events was taken as an estimate of the hemodynamic response function (HRF) for each subject (Figure S3a). We observed that our subjects differed in the overall amplitude of their BOLD fMRI HRF. We obtained the peak amplitude of the HRF for each subject, and then divided each value by the mean of the values across subjects. We treated the result as a "subject scaler" that was used to normalize subsequent measurements of response amplitude from each subject to remove this individual difference.

The evoked response for each spectral-pulse stimulus type for each subject was then modeled with a two-parameter model (Figure S3b). The first parameter controlled the duration of a step-function of neural activity that was then convolved by the HRF for the subject. The resulting shape of BOLD fMRI response was normalized to have unit amplitude, and then subjected to a gain parameter. The best fitting parameters (in the least-squares sense) were found by non-linear search (`fmincon` in MATLAB).

We conducted whole brain (cortical surface) analysis of the data from Experiments 1 (400% melanopsin only) and 2 (400% LMS only). The time-series data from each voxel for each subject was projected to hemisphere-symmetric cortical surface atlas (`fsaverage-sym`) and smoothed on the cortical surface using a 5 mm FWHM Gaussian kernel. An approximation to a Fourier basis set analysis was conducted on the time-series data at each cortical point for each of the k scan runs using the FSL FEAT and FOBS routines, modeling the 14 s period following each stimulus event with a set of 14 sinusoids that varied in frequency from half a cycle per period to 14 cycles per period. The p-value associated with the F-statistic for this model was obtained at each vertex. For each subject and hemisphere (at each cortical point), the set of p-values across the k scan runs were used to calculate a χ^2-value with $2k$ degrees of freedom using Fisher's method. The map of p-values corresponding to the χ^2 map from each subject and hemisphere were combined again using Fisher's method, and the resulting maps of χ^2-values were used to illustrate the evoked stimulus effect shown in Figures 2a, b. These maps were thresholded at a value of $\chi^2(\text{df} = 16) = 61.4$. This corresponds to a Bonferroni corrected, map-wise $p = 0.05$ threshold after accounting for the number of vertices in the group map (and disregarding map spatial smoothness).

Eye and pupil tracking. Infrared (IR) video eye-tracking was performed during Experiments 4 and 5. The LiveTrack AV MR-compatible eye tracking camera (Cambridge Research Systems, Rochester, UK) was used to record video from the left eye of each subject at either 60 Hz or 30 Hz (the lower frame rate was used in the Mel CRF studies for ASO and GKA, and in the LMS CRF study for ASO). The camera was attached to the 64-channel head coil using a custom mount, and positioned 10–15 cm away from the left eye of the subject. The camera and head coil were draped in black felt to minimize scattering of light to the left eye from the eyepiece over the right eye. Consistent with the minimization of scattered light and room light, subjects generally reported binocular suppression of the left eye during these experiments.

A live video feed from the system was used to monitor subject alertness and head motion during scanning. The system recorded the position of the IR glint on the tear film and the size and position of an ellipse fit to the outline of the pupil in each frame, and from this derived pupil size and eye position. We found that the automated ellipse fitting was unstable in the vertical dimension. For this reason, we report here the pupil size derived from the horizontal width of the fitted ellipse, and eye position in the horizontal plane only. The timing of data collection was synced with MRI scan acquisition and stimulus presentation using a TTL signal sent by the scanner at the start of the scan and at the time of each image repetition (TR). Absolute pupil size was determined by calibrating the camera against targets of known dimension following each scan session.

The analysis pipeline for the pupil and eye position data is available on GitHub (`https://github.com/gkaguirrelab/pupilMelanopsinMRIAnalysis`). First, blinks were identified as timepoints during which the glint was not visible. The pupil size and position measurements were set to `NaN` in the 50 ms before and after each blink. The pupil size vectors were then subjected to a 0.025 Hz high-pass filter. A 13 s period of pupil response following the onset of every trial was extracted, expressed in percent change units, and set to have a value of zero during the first 100 ms following the onset of the stimulus. The median response across trials for each stimulus type for each subject was obtained (Figure S8). Each median response was then fit with a six-parameter, three-component pupil temporal model (Figure S9) using a non-linear search (`fmincon` in MATLAB) within a temporal fitting engine (`https://github.com/gkaguirrelab/temporalFittingEngine`).

We observed that our subjects differed in the overall amplitude of their pupil response. For each subject, we obtained the total area of pupil response (% change × seconds) across all stimulus types (Mel and LMS pulses of every contrast level). We divided each value by the mean of the set of values across subjects. We treated the result as a "subject scaler" that was used to normalize measurements of response amplitude from each subject to remove this individual difference.

Perceptual rating experiment. Perceptual ratings were obtained using the same stimulus presentation apparatus as was used in the fMRI

experiments. Subjects were positioned in a chin rest in a darkened room and observed stimuli with their pharmacologically dilated right eye. The experiment was composed of several periods. In each period, the subject would first adapt to a stimulus background, and then view spectral pulses of a particular stimulus type (light flux, LMS, or melanopsin). Three initial "exposure" periods were used to familiarize subjects with the procedure and the perceptual range of the stimuli. Each exposure consisted of 1 min of adaptation to the background, followed by presentation of 3 spectral pulse trials of a given type. Subjects were asked only to observe the stimuli. Following the exposure periods, the subject participated in six "rating" periods. Each rating period consisted of a 5 min adaptation to a background, followed by the presentation of 9 spectral pulse trials of a given type. Before each trial, the subject was read a description of a perceptual property that they were to rate for the upcoming stimulus trial. Following presentation of the stimulus pulse, the subject was prompted for their rating on a scale of 1 to 7. The subject could ask for the description and pulse to be repeated one additional time prior to providing a rating. The subject was asked to rate a different perceptual property for each of the 9 trials in a given rating period. Rating periods for light flux, LMS, and melanopsin stimuli were each conducted twice, with subjects randomized to follow one of two trial orders:

i. light flux, melanopsin, LMS, light flux, melanopsin, LMS

ii. light flux, LMS, melanopsin, light flux, LMS, melanopsin

The nine perceptual properties were defined by pairs of antonyms (e. g., cool–warm) that defined the extreme ratings of 1 and 7. Subjects were instructed to fixate the center of the stimulus field and report the appearance of the light pulse in visual periphery, doing their best to ignore any percept within or adjacent to the obscured macular region.

For the perceptual rating experiment, our photoreceptor spectral sensitivity estimates assumed a 27.5° field for generating the receptor-isolating modulations while the observed field was in fact 64° as in the fMRI experiments. This lead to numerical but insignificant differences in the estimate for the macular pigment density. In the contrast and splatter calculations for this experiment, we assumed the 64° in our estimates for the spectral sensitivities.

The first two dimensions of the principal components analysis of the perceptual rating data were used to describe the results as the addition of further dimensions was found to reduce cross-validated categorization accuracy.

Spectrum seeking to improve stimulus control. The stimuli used in the perceptual study were subjected to an additional refinement prior to each data collection session, designed to further reduce inadvertent cone contrast in the melanopsin-directed stimulus. An adaptive spectrum-correcting procedure addressed uncertainty in our device calibration due to instrumental drift and small failures of primary additivity. This procedure adjusted the mirror settings in our digital light synthesis engine so as to match the nominal, receptor-isolating spectra. This procedure was performed for the age-adjusted stimuli of all subjects in the perceptual rating experiment.

We started with a pair of primary values designed to yield a certain contrast: The background primary values P_{BG} and the modulation primary values P_{Mod}. The spectral calibration procedure of the light synthesis engine determines the primary matrix M, which, when multiplied with the primary values and added to the dark spectrum spd_{dark}, yields the predicted target spectra $spd_{\mathrm{BG,\,target}}$ and $spd_{\mathrm{Mod,\,target}}$. Contrast properties of the stimulus are defined with respect to these two spectra.

During a validation, we gamma-correct the linear primaries values, P using our device calibration model. This yields the pair of settings S_{BG} and S_{Mod}. These are then provided to the light engine and spectral measurements $spd_{\mathrm{BG,\,val}}$ and $spd_{\mathrm{Mod,\,val}}$ are obtained. Due to imprecision in the stimulus control, $spd_{\mathrm{BG,\,target}}$ and $spd_{\mathrm{BG,\,val}}$, and $spd_{\mathrm{Mod,\,target}}$ and $spd_{\mathrm{Mod,\,val}}$, are different.

The goal of the adaptive procedure is to find terms ΔP_{BG} and ΔP_{Mod} which correct the primary values. To do this, we do the following ($i \in 1 \ldots N$, where typically $N = 10$):

i. Perform gamma correction: $P_{i,\,\mathrm{BG}} \rightarrow S_{i,\,\mathrm{BG}}$ and $P_{i,\,\mathrm{Mod}} \rightarrow S_{i,\,\mathrm{Mod}}$.

ii. Obtain target spectra: $P_{1,\,\mathrm{BG}} \rightarrow spd_{\mathrm{BG,\,target}}$ and $P_{1,\,\mathrm{Mod}} \rightarrow spd_{\mathrm{Mod,\,target}}$.

iii. Measure $spd_{i,\,\mathrm{BG,\,val}}$ and $spd_{i,\,\mathrm{Mod,\,val}}$.

iv. Calculate the spectral difference between target and validated spectra in the i-th iteration: $\Delta spd_{i,\,\mathrm{BG}} = spd_{\mathrm{BG,\,target}} - spd_{i,\,\mathrm{BG,\,val}}$ and $\Delta spd_{i,\,\mathrm{Mod}} = spd_{\mathrm{Mod,\,target}} - spd_{i,\,\mathrm{Mod,\,val}}$.

v. Obtain $\Delta P_{i,\,\mathrm{BG}}$ and $\Delta P_{i,\,\mathrm{Mod}}$ corresponding to the spectral differences using our calibration model that maps spectra back to device coordinates.

vi. Update the primary values for the next iteration: $P_{i+1,\,\mathrm{BG}} = P_{i,\,\mathrm{BG}} + \lambda \Delta P_{i,\,\mathrm{BG}}$ and $P_{i+1,\,\mathrm{Mod}} = P_{i,\,\mathrm{Mod}} + \lambda \Delta P_{i,\,\mathrm{Mod}}$, where $\lambda = 0.8$ is the learning rate.

We find that this spectrum-correction procedure reliably reduces inadvertent cone stimulation due to uncertainty in device control.

Data and code availability. All raw data are available as packaged and MD5-hashed archives as well as tables detailing the biological variability on FigShare (https://figshare.com/s/0baea6ed50758abbabf4). All code is available in public GitHub repositories (https://github.com/gkaguirrelab/Spitschan_2017_PNAS/). Un-thresholded statistical maps from Experiments 1 and 2 for each subject are available from NeuroVault (https://neurovault.org/collections/2459/).

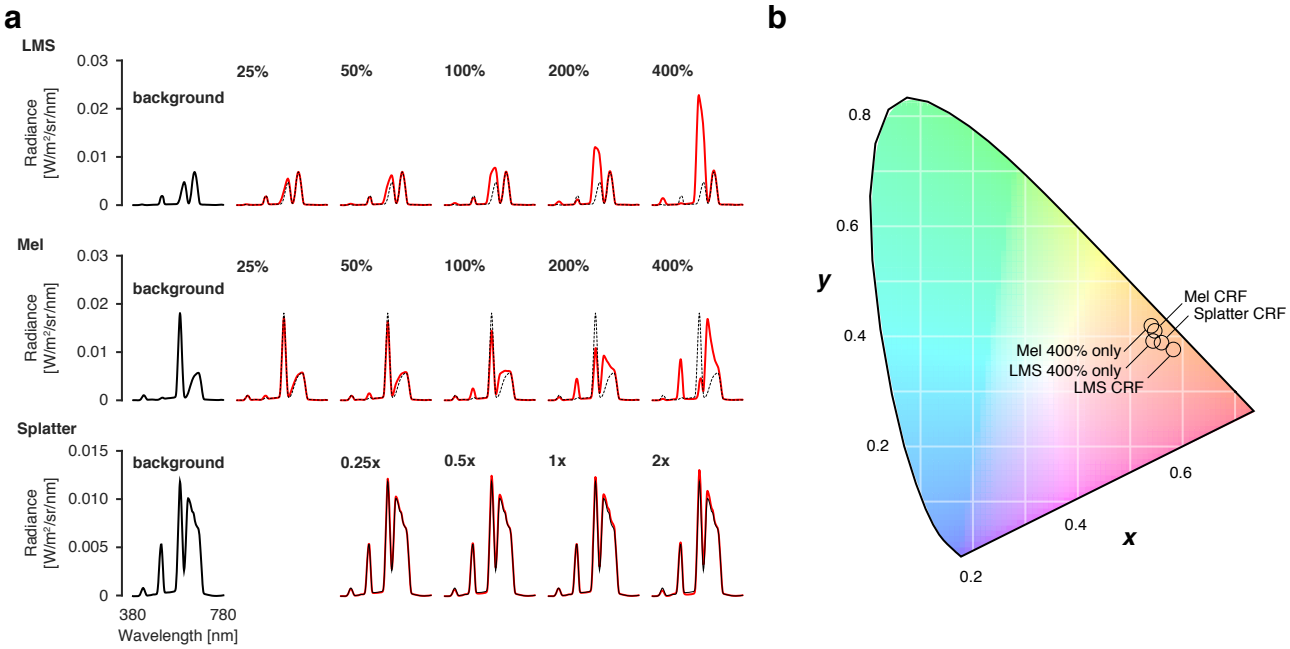

Fig. S1. Spectra and chroma of all stimuli (related to Figure 1). *(a)* The stimulation spectra (red) for each contrast level in comparison to the background spectrum (black) for the LMS, melanopsin, and splatter stimuli. *(b)* The calculated CIE 1931 chromaticity (24) for all stimulus backgrounds. Experiments that presented stimuli of different contrast levels are indicated with "CRF" (Contrast Response Function).

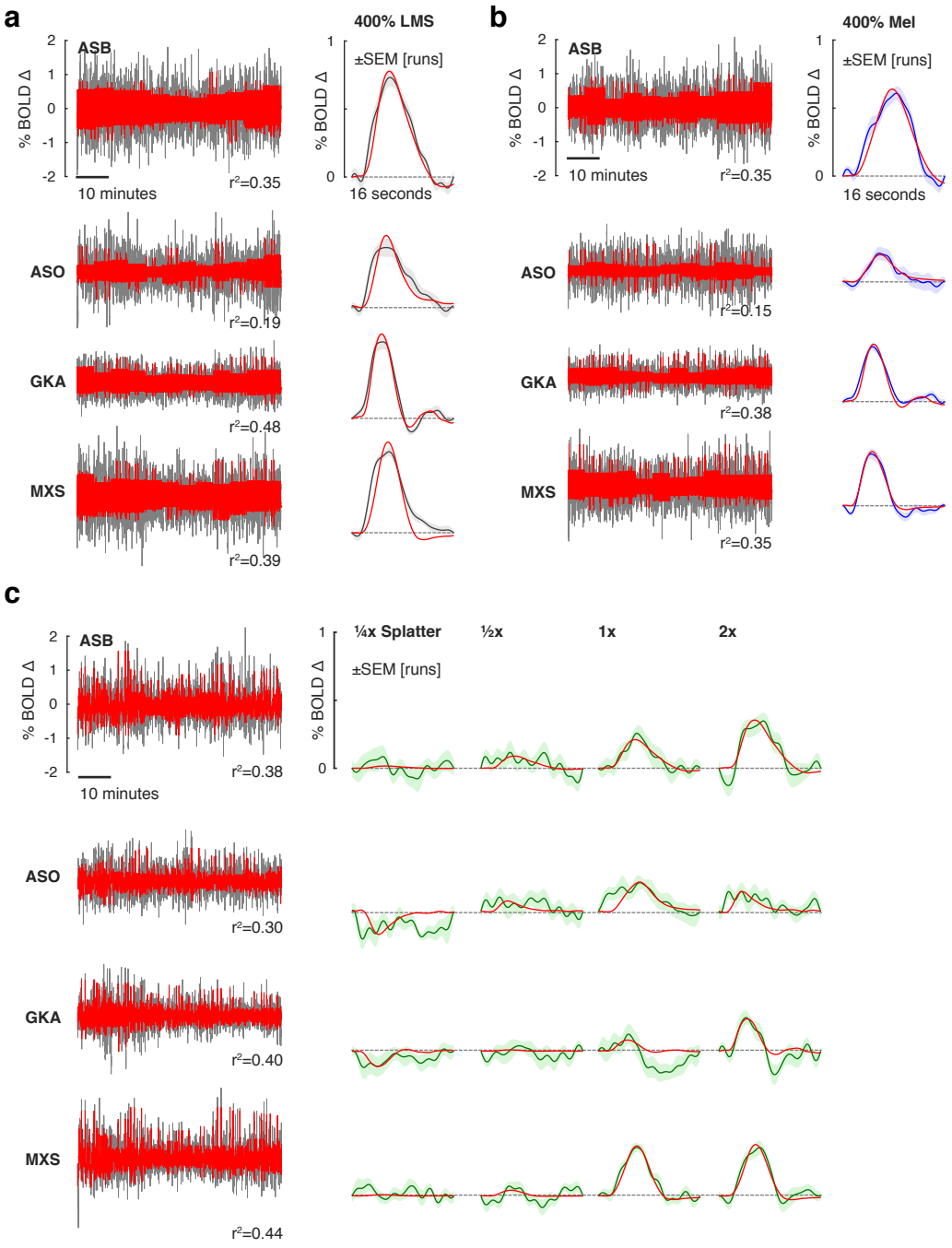

Fig. S2. Additional BOLD fMRI time-series and model fits (related to Figure 2). *(a)* V1 responses to 400% LMS stimulation. Our initial study to explore broad cortical responses presented only trials with 400% stimulus contrast. *Left* The BOLD fMRI time-series data from the area V1 region for each subject (black), following pre-processing to remove nuisance effects. A Fourier basis set modeled (red) the mean evoked response to each contrast level during each run with the r^2 values of the model fit indicated. *Right* The evoked responses for each subject to the 400% LMS stimuli (black), and SEM of the response across the 9-10 scanning runs performed in each subject (shaded region). The responses were fit by a model (red) that convolved a step function of neural activity by the hemodynamic response function measured for each subject. *(b)* The corresponding responses within the V1 region to melanopsin stimulation of 400% contrast. *(c)* The corresponding responses within the V1 region to the "splatter" modulation, with contrast varying from one-quarter to two-times the estimated cone splatter contrast arising from device imprecision (Figure S5).

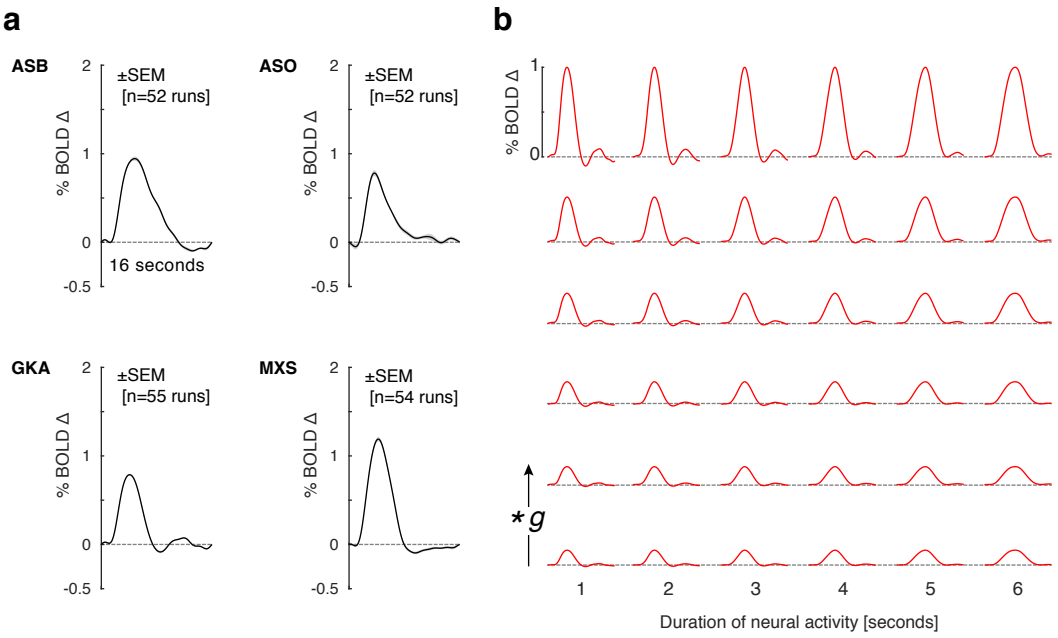

Fig. S3. HRFs and evoked response model (related to Figure 2). *(a)* In all experiments, ~14% of stimulus trials were randomly replaced with an attention event, during which the stimulus dimmed for 500 ms and in response to which the subject was to press a button on a response pad. The same response events occurred in each of the >50, 336 second scan runs for each subject across all experimental conditions. The BOLD fMRI response evoked within the studied V1 region in response to the attention events was estimated using a Fourier basis set for each run for each subject. The 16 s that followed each event was modeled with 8 harmonics, providing a temporal resolution of 1 Hz. The average response across runs (black) for each subject (expressed in units of percent BOLD signal change) was taken to be an estimate of the hemodynamic impulse response for that subject and was used in modeling of fMRI responses to other stimulation conditions for that subject. The SEM of the response across runs (shaded gray) is in most cases smaller than the plot line. *(b)* Shown are how the predicted BOLD fMRI responses for subject GKA vary with inferred duration of neural activity (across each row) and amplitude of BOLD fMRI response (each row shows a different value of *g*). The model varied the duration of a step function of neural activity that was then convolved with the HRF for that subject and subjected to multiplicative scaling (∗*g*) to best fit the evoked response. The fits provided by this model are shown in Figure 2 and Figure S2, and the amplitude and duration parameters derived from fitting are the subject of Figures 3 and S4.

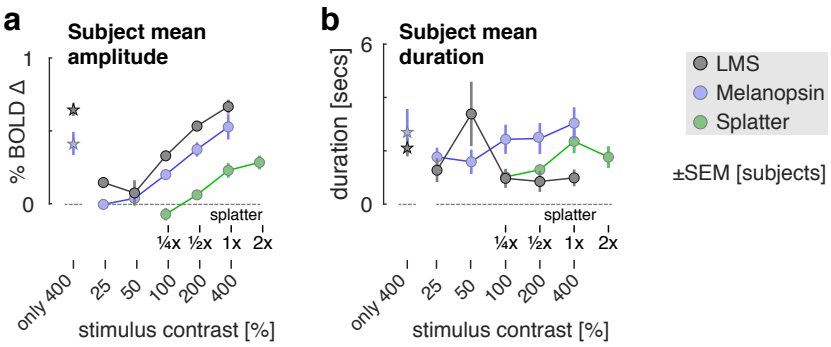

Fig. S4. Amplitude and duration of response in V1 by stimulus contrast (related to Figure 3). *(a)* The mean amplitude of evoked response with the V1 region across subjects for each contrast level is shown for the LMS (gray), melanopsin (cyan), and "splatter" (green) stimulus conditions. The star symbols are the amplitude measurements obtained in the initial, 400% contrast only LMS and melanopsin studies. The 1x splatter condition presented cone contrast equal to the maximum inadvertent contrast measured in validated spectra in the melanopsin and LMS experiments. We calculated as well the amplitude of response for the 400% contrast only LMS and melanopsin studies within visual areas V2 and V3 (for which we have available an eccentricity map from cortical anatomy (22)). Within area V1, the response amplitudes (± across subjects) were 0.6459 ± 0.1000 and 0.4123 ± 0.1799 for LMS and melanopsin, respectively. Within V2 the values were 0.2675 ± 0.1177 and 0.3684 ± 0.0842 (LMS and melanopsin), and within V3 they were 0.2531 ± 0.1242 and 0.3790 ± 0.0657 (LMS and melanopsin). Overall, the response to wide-field LMS stimulation declined across visual areas (as reported previously (25)) while the response to melanopsin was more evenly maintained across these early visual areas. *(b)* The mean modeled duration across subjects of underlying neural activity within the V1 region is shown for the three stimulus conditions.

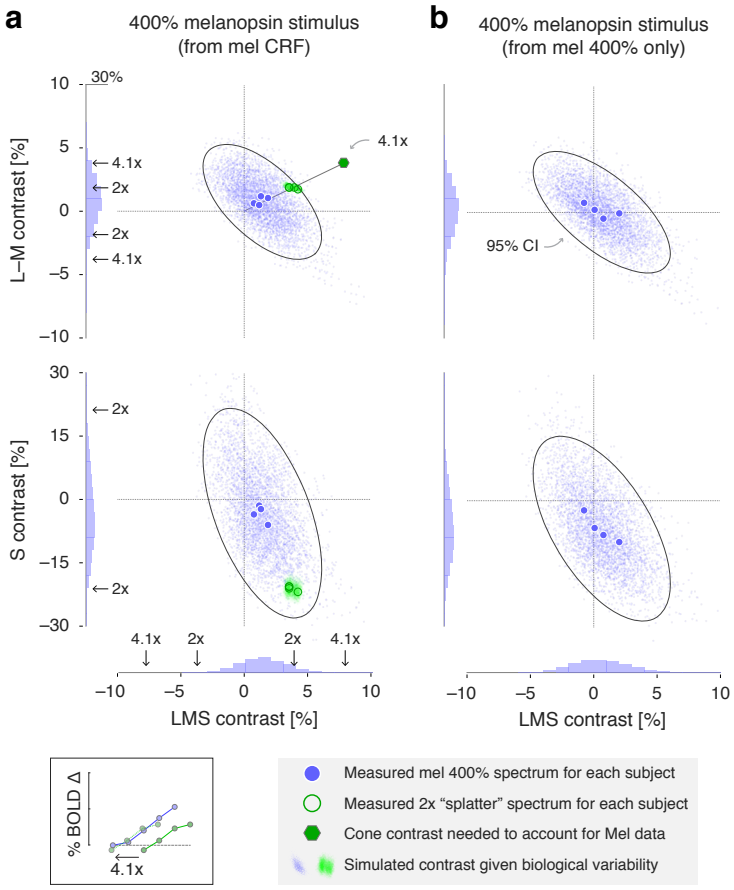

Fig. S5. Inadvertent cone contrast in the fMRI stimuli (related to Figure 3). *(a)* Due to biological variability and inevitable imperfections in device control, a nominally cone silent modulation will produce inadvertent contrast upon the cones. We considered the extent to which this undesired contrast could account for the BOLD fMRI signals we observed in response to a melanopsin-directed spectral pulse. For each subject, multiple measurements of the 400% melanopsin-directed stimulus spectrum were made before and after each data collection session. This set of measurements was averaged for each subject to produce a single spectrum, which was then submitted to a calculation (https://github.com/spitschan/SilentSubstitutionToolbox) that estimated the degree of contrast upon each of the postreceptoral cone mechanisms (L–M, S, LMS). The four large, blue circles in each plot indicate the calculated contrast caused by device imprecision for the stimuli seen by each of the observers.

We created a stimulus modulation ("1x splatter"; Figure S1a) that had cone contrast equal to the max, across-subject contrast attributable to device imprecision. A set of "splatter" stimuli with log-spaced intensity ($\frac{1}{4}\times$, $\frac{1}{2}\times$, $1\times$, $2\times$) were derived from this initial modulation and studied during a control BOLD fMRI experiment. The spectrum of the 2x modulation was measured for each experimental session for each subject, and the cone contrast estimated in this modulation is indicated by the large, green circles (one circle for each observer; some plot symbols are overlapped).

We next considered how biological variability could cause these estimates of cone contrast to change. Our model of cone contrast incorporates assumptions regarding: lens transmittance; density of macular pigment; L, M, and S cone density; and variation in the peak spectral sensitivity ($\lambda_{\max}$) of the L, M, and S cones. We simulated biological variation in these parameters by conducting 1,000 re-calculations of the cone contrast for each subject, using values for each parameter drawn from published distributions of individual differences (6). The cone contrast returned by each simulation comprises a point in the cloud of blue values in each plot; an ellipse (solid line) indicates the iso-probability contour that encloses 95% of the 2D projection of the bootstrapped values upon the postreceptoral axes, computed assuming that the underlying distribution was a bivariate Gaussian. The marginal distribution of this set of simulated contrast values is shown on each cardinal axis. The same calculation was conducted for the 2x splatter spectra, yielding the cloud of green points. We next related these values to our BOLD fMRI measurements. We have for each subject a contrast response function (CRF) for melanopsin and for multiples of inadvertent cone contrast (splatter) due to device imprecision (Figure 3). For each subject, we asked how much larger the splatter contrast would have to have been to produce responses that match the melanopsin CRF; this amounts to asking how many log-units the splatter CRF must be shifted to the left to best match the melanopsin CRF (inset, bottom left). Across subjects, the mean shift multiplier was 4.1 (individual values were ASB 3.2, ASO 2.8, GKA 7.7, MXS 4.1). Extending the line that connects the origin of the cone-contrast space and the $2\times$ splatter modulation, we identified the position that would correspond to a $4.1\times$ splatter modulation (green hexagon). We considered the position of this point (and its mirror symmetric reflections) in the opponent modulation space with respect to the marginal distributions of simulated inadvertent contrast due to biological variability and device imprecision. The key observation is that the inadvertent cone contrast necessary to produce the observed BOLD fMRI responses to the 400% melanopsin stimulus are unlikely to have occurred. The proportion of simulated contrast values (in both tails) that exceed the $4.1\times$ level is 0.2% on the LMS dimension; 0% on the S dimension; and 5.3% on the L–M dimension. To account for our data, one or more of these values would have to have been exceeded for all four subjects. The odds of this occurring for a single subject is: $P(\text{LMS or L–M exceeded}) = 1 - ((1 - 0.053) \times (1 - 0.002)) = 0.0549$ and the odds of this occurring for all four subjects is $p = 9.1 \times 10^{-6}$. *(b)* The corresponding calculation of cone contrast due to device imprecision and biological variability for the melanopsin stimulus used in the 400% contrast only experiment.

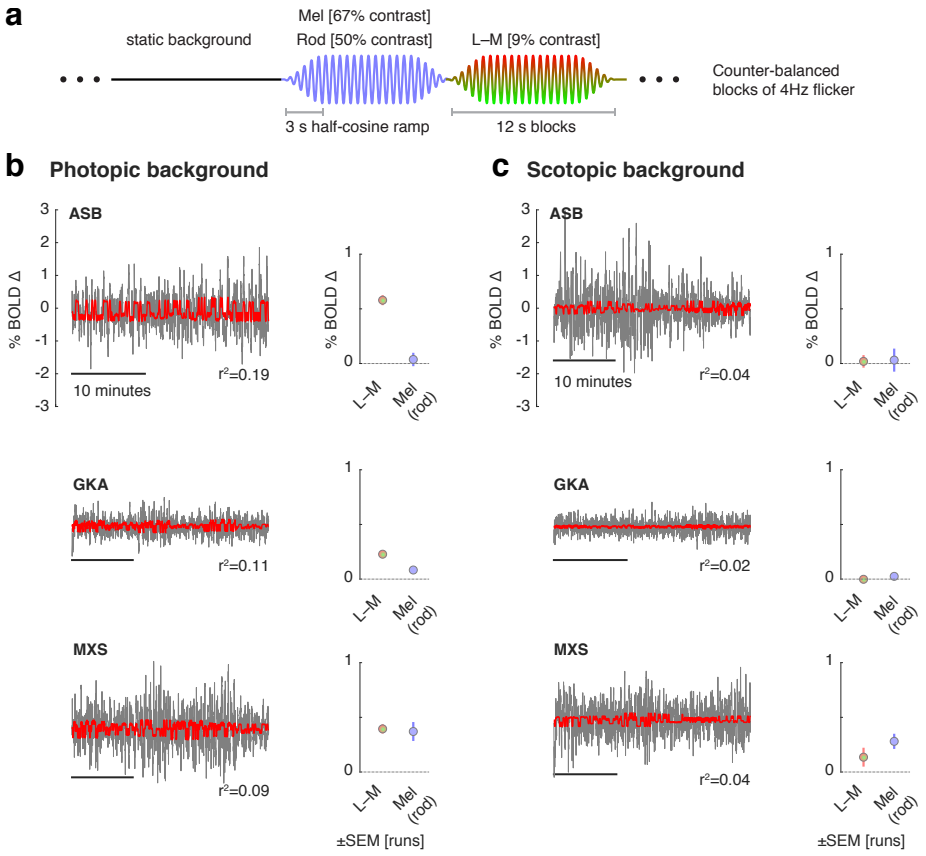

Fig. S6. An unsuccessful control experiment (related to Figure 3). The rod and melanopsin spectral sensitivity functions overlap extensively. The background used for our melanopsin directed stimuli was 3.5 $\log_{10}$ scotopic trolands (sc td), nominally at or above the rod saturation threshold, found to be 3.0 $\log_{10}$ sc td (Fig. 2 of Adelson, 1982 (26)) or 3.3–3.7 $\log_{10}$ sc td (Aguilar & Stiles, 1954 (27)). Therefore, we may expect in our experiments that there is no, or minimal, time-varying signal contributed by the rods. Nonetheless, we considered control experiments that could address the possibility of rod intrusion. While it is possible in principle to create a melanopsin directed stimulus that silences both the rods and cones, in practice we find that our device is limited to a maximum 60% unipolar (Weber) contrast pulse directed at melanopsin while silencing both rods and cones. Given our finding that at least 100% unipolar melanopsin contrast is needed to produce a reliable cortical response, we regarded this stimulus as ineffective. Instead, we examined whether the response to our melanopsin directed stimulus varied as a function of temporal frequency, with the logic that melanopsin responses would be attenuated to a stimulus modulated at 4 Hz, while rod responses would persist. Ultimately we found this experiment to be uninformative. The BOLD responses evoked by the stimuli were small and/or poorly modeled, with low r^2 values, particularly in the scotopic condition. Moreover, inconsistent responses were obtained across subjects. Despite our inability to draw clear conclusions from these measurements, we present the data here for completeness. *(a)* The experimental design was adapted from a prior study (2). Around a common background, we presented a 4 Hz modulation that targeted either L–M with a 9% bipolar (Michelson) contrast (while silencing the rods) or melanopsin with 67% bipolar contrast on melanopsin and 50% bipolar contrast on rods. The modulations were presented in 12 s blocks, with a 3 s half-cosine window at onset and offset, in a counter-balanced order. *(b)* Photopic conditions. *Left* The BOLD fMRI time-series data from the area V1 region for each subject (black), following pre-processing to remove nuisance effects. The data were modeled (red) with a step-function for each stimulus condition, convolved by subject-specific hemodynamic response function. *Right* The amplitude of evoked responses for each subject for the 4 Hz L–M and melanopsin modulation blocks as compared to the static background. *(c)* The corresponding data obtained during scanning under scotopic conditions. Subjects dark-adapted for at least 20 minutes prior to scanning. A 6 log unit neutral density filter was placed in the light path, reducing the stimulus background to approx. 0.0001 cd/m^2.

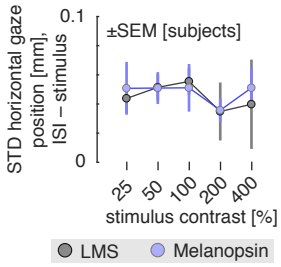

Fig. S7. Variation in horizontal gaze position with stimulation (related to Figure 4). A prior functional MRI study that presented a 50% Weber contrast melanopsin modulation did not find responses within the visual cortex, but did observe BOLD fMRI responses within the frontal eye fields (28). The authors speculated that melanopsin stimulation produces changes in alertness that manifest as these cortical responses, although eye movements were not recorded during their study. In our whole brain analysis (Figure 2a, 2b) we find responses within the frontal eye fields for both the luminance and melanopsin pulses at lowered map thresholds (unthresholded maps available from https://neurovault.org/collections/2459/). We considered the possibility that our stimulus pulses might cause subjects to briefly increase or decrease saccadic eye movements. Subjects were asked to maintain fixation upon the center of a 5° opaque circle. Infrared video of the left eye was recorded during functional MRI scanning in some experiments. We measured the horizontal position of the eye during the scanning session to examine if stimulus presentation led to systematic changes in fixation stability. While vertical eye position was recorded, these data were not considered given that the eye has less fixational variation in the vertical plane, and the generally noisier quality of the vertical position data. The standard deviation of eye position was measured during the three seconds of stimulus presentation and during the ensuing interstimulus interval (ISI). The mean difference (averaged across subjects) between the ISI and stimulated periods was obtained for the LMS (gray) and melanopsin (blue) stimuli at each contrast level. Subjects consistently reduced eye movements during the luminance and melanopsin stimulation periods as compared to the inter-stimulus-interval. This effect may account for the frontal eye field responses in our data and in the prior report (28). As eye movements alone can evoke responses in visual cortex (29), we considered that a systematic difference in eye movements across contrast levels might confound our finding of a contrast-dependent response in area V1. However, no eye movement difference was seen as a function of contrast level or stimulus type (LMS vs. melanopsin).

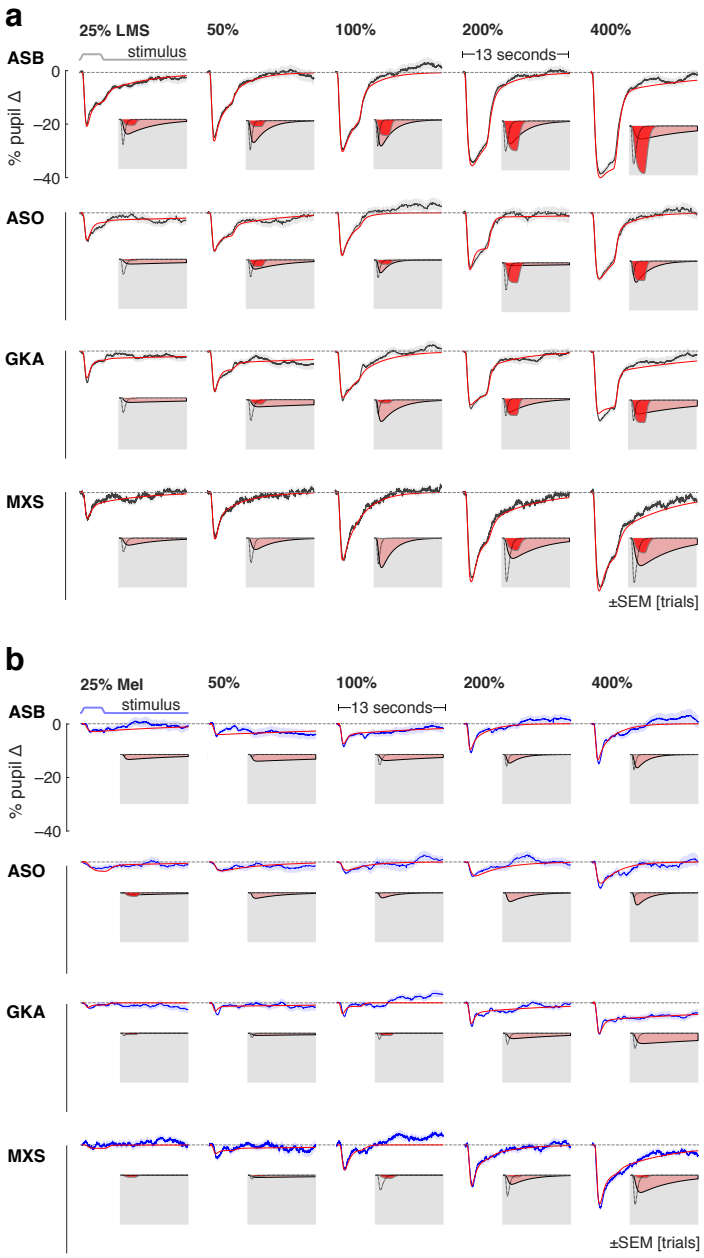

Fig. S8. Individual subject pupil responses (related to Figure 4). The consensual pupil response of the left eye was measured during stimulation of the pharmacologically dilated right eye. *(a)* The mean (across trials) pupil response evoked by LMS stimulation of varying contrast levels (black), with SEM across trials (shaded). Each row contains the data from a different participant. The evoked response was fit with a three component, six-parameter model (red). The three components that model each response are shown inset on a gray field. *(b)* The corresponding mean pupil responses evoked by melanopsin stimulation of varying contrast levels.

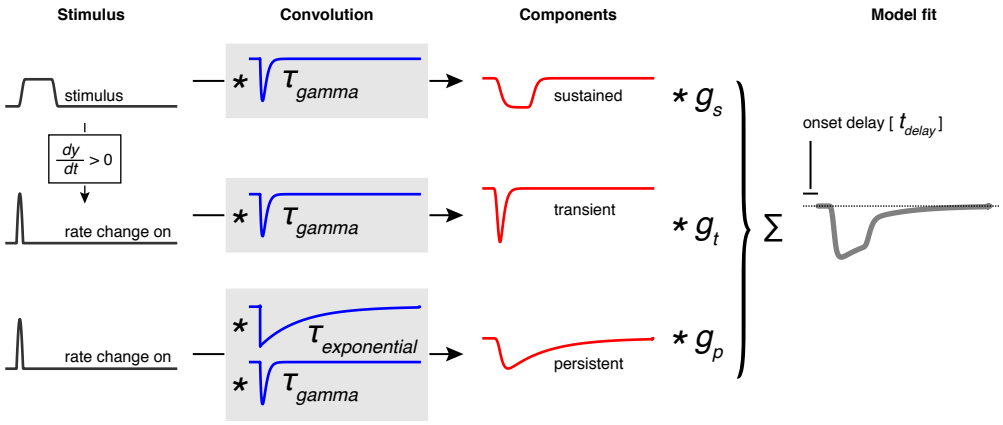

Fig. S9. Pupil temporal model (related to Figure 4). The across-trial, within-subject average evoked pupil response to each stimulus type (LMS and melanopsin) and contrast level was fit with a six-parameter, three-component model using a non-linear temporal fitting engine (https://github.com/gkaguirrelab/temporalFittingEngine). The model was designed to capture the three, visually apparent and temporally separated components of the evoked pupil response. The elements of the model are not intended to directly correspond to any particular biological mechanism. The input to the model was the stimulus profile (black). An additional input vector, representing the rate of stimulus change at onset, was created by differentiating the stimulus profile and retaining the positive elements. These three vectors were then subjected to convolution operations composed of a gamma and exponential decay function (blue), each under the control of a single time-constant parameter (τ_{gamma} and $\tau_{\text{exponential}}$). The resulting three components (red) were normalized to have unit area, and then subjected to multiplicative scaling by a gain parameter applied to each component ($g_{\text{transient}}$, $g_{\text{sustained}}$, and $g_{\text{persistent}}$). The scaled components were summed to produce the modeled response (gray), which was temporally shifted (t_{delay}). We observed that some evoked responses for some subjects had a late dilation phase in which the pupil became larger than its baseline size. We did not attempt to capture this inconsistent behavior in our model.

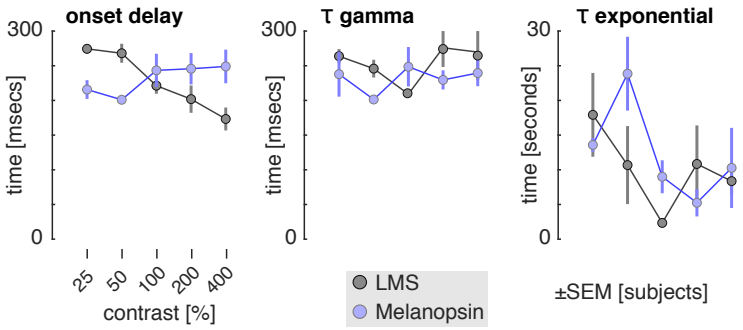

Fig. S10. Temporal pupil model parameters by contrast (related to Figure 4). Pupil responses were fit with a six-parameter model, of which three parameters controlled the temporal behavior of the model. Each plot presents the mean (across subjects) of a temporal parameter, as a function of contrast for LMS (gray) and melanopsin (blue) stimulation.

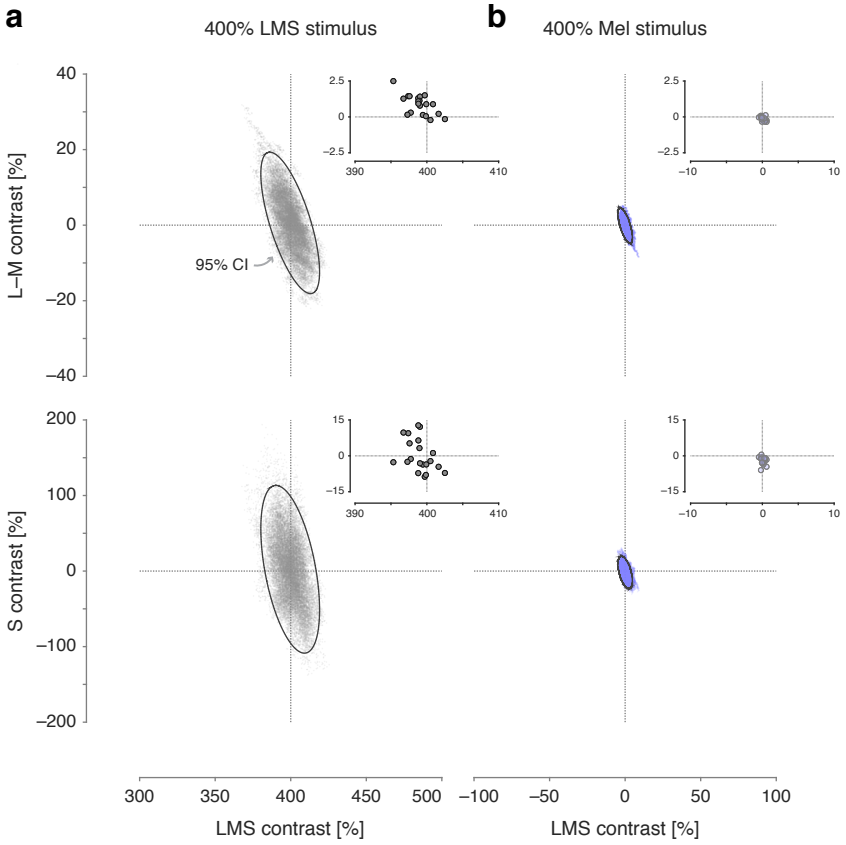

Fig. S11. Inadvertent cone contrast in the perceptual stimuli (related to Figure 5). *Inset* in each plot is the calculated postreceptoral cone contrast of the melanopsin and luminance 400% spectral pulses used in the perceptual experiment. Each point corresponds to the difference between the background and stimulus spectra measured for each subject at the time of their testing session. Following the same procedure as described in Figure S5, we then simulated the postreceptoral cone contrast that might be produced by our stimuli in the face of biological variability in our subjects. *(a)* Postreceptoral contrast estimated from simulations for the 400% LMS (luminance) stimulus. *(b)* Postreceptoral contrast estimated from simulations for the 400% melanopsin stimulus.

Table S1. Across-subject ratings of nine perceptual qualities for 400% contrast pulses of the three stimulus types.

	Melanopsin	*LMS*	*Light flux*
quality	median ± inter-quartile range		
cool to warm	4.25 ± 4.00	4.50 ± 2.00	4.50 ± 1.25
dull to glowing	4.50 ± 3.75	5.00 ± 1.25	5.50 ± 2.50
colorless to colored	5.75 ± 1.25	3.25 ± 2.25	2.00 ± 1.50
focused to blurred	5.00 ± 1.75	3.50 ± 3.00	3.50 ± 2.25
slow to rapid	4.00 ± 2.50	4.75 ± 2.00	4.50 ± 1.75
pleasant to unpleasant	4.75 ± 2.75	3.00 ± 2.00	3.00 ± 1.50
dim to bright	2.50 ± 3.25	5.25 ± 1.50	6.00 ± 1.25
smooth to jagged	3.50 ± 2.75	2.25 ± 1.75	2.00 ± 1.50
constant to fading	5.00 ± 2.50	2.00 ± 1.75	2.00 ± 1.50

Table S2. Free-form descriptions of the pulsed stimuli. Subjects in the perception experiment were invited to describe their impressions of the stimuli during a debriefing session and these were recorded by the examiner. Subject ID codes given in parentheses. The subject was not told the spectral identity of the stimuli, and in their descriptions referred to the stimuli by their experimental order; these references to run order are replaced here by the spectral identity of the stimulus for clarity. Some subjects provided descriptions of changes in the appearance of the stimulus at the edge of the masked macular region; they were asked to ignore this aspect of the stimulus in their ratings.

Melanopsin
Lot of difference between surrounding of dot (fixation dot) and periphery. Space around dot, red-orange to lighter orange. Cloudy thing around dot, ignoring it for periphery. Difference between center and periphery large and distracting. Looks like a lava lamp. Lava changes shape between pulses. (MELA 0026)
Appeared distinctly red – maxwell spot appeared very red. Faded to the black that is the noise when your eyes are closed about a dots (fixation dot) width away from the center. (MELA 0037)
Definitely looks reddish around the ring of the fixation dot, further into the periphery not so much. Hard to describe. (MELA 0038)
Pulses were disorienting. Kind of like if you got hit in the head really sharply. Experience kind of like flashing lights and fade out. Pulses were more green than other two types of runs. Other two runs were orange-ish. (MELA 0043)
Huge transition from background to pulse. Went from a yellow to grey color, but the pulse still contained color aspects of the background. (MELA 0049)
Pulse was so gradual that couldn't tell it's changing color. Felt a bit like the pulse was straining their eye compared to the background. Pulses looked pink-red and magenta. (MELA 0073)
Like a psychedelic; unnatural; stimulus that they rarely experience. The psychedelic and foreign, less familiar. More shimmering, corresponds to psychadelicness. (MELA 0074)
Looked more different than the other two (light Flux and LMS). Background was green, pulse was closer to red. Harder to focus on too.Green background was red towards the middle. Less harsh than first time seen. (MELA 0075)
Did see maxwell spot extend beyond the edge of the black fixation dot. Pulse was very strange color – did not know what color it was. Trouble describing color. (MELA 0080)
Pulses looked similar to each other, appeared green. Pulses has same brightness and same onset time. (MELA 0081)
Like looking at the sun. Coloration looks like the sun, NOT uncomfortable. Felt like a faded version of sun. (MELA 0082)
Like blinding in a sense. Switches between white and black, not uncomfortable. Not really any color. (MELA 0088)
Very similar in color to first run, but the onset is different against background. Background seems different: looks like it has less color, says they know it is orange but it looks more bland in the first run. (MELA 0090)
Fairly unpleasant. Seemed really harsh, like staring at something really bright. Automatically wanted to blink. uncomfortable but not painful. Discomfort because of brightness. Really aversive, super harsh. Made them want to blink. Very bright. (MELA 0094)
LMS
See a very thin but very bright ring around black circle, very red. Red ring still there, becomes more defined longer they stare at background. (MELA 0026)
lighter version of peach stimulus. Seemed more faded along edges. Seemed similar to pulse before last (Light Flux). (MELA 0037)
Uniform, sort of whitish pulse/intensity change (MELA 0038)
Started off as background, seemed like Light flux background, but by the third rating (colorless to colored) background seemed yellow with pink pulse. Seemed like a less bright version of Light Flux. The background remained yellow with specks of pink. Adaptation was yellowish in hue. (MELA 0049)
If compared to first pulse, less brightness, color didn't change as much and more dull. Seemed clearer but less bright. (MELA 0050)
Seems like the pulse is a cooler, lighter version of the background. Comfortable to look at. Was cooler than background and more white-toned than background. White toned meant the pulse was faded to a lighter version of the background, the brightness was different. (MELA 0073)
Pretty comforting, benign, friendly, familiar. Strong but comfortable, very luminous. (MELA 0074)
Looked similar to light flux in terms of color but dimmer. Like last run (Light flux) but not as bright, seemed less harsh. (MELA 0075)
Focused to blurry is difficult: didn't notice any particular focusedness or blurriness. (MELA 0077)
Perceived it as the same as Light Flux. Seemed similar to other runs except Mel. (MELA 0080)
Pulses were all the same color and brightness, did not state what color pulses were. Pulses appeared identical. (MELA 0081)
Like the first run (Light flux) but better. Felt like it was hazy or foggy. Color was the same, just foggy. Eye piece was not foggy. (MELA 0082)
Kind of brownish gray pulse. Kind of colorless, similar to last run (LF) (MELA 0088)
Feeling desensitized to brightness, these pulses didn't seem as bright as first time though the color was the same. (MELA 0090)
Roughly similar to first pulse – less colorful than first one in terms of absolute color. Most other aspects seemed pretty similar. Looks neutral like other rounds. Very bland and pastel-ish. (MELA 0094)
Light flux
Pulse looked peachish in color. More pinkish than first run LF and run 1 LMS. (MELA 0037)
Looked like a uniform whitish intensity increase, nothing really stood out. (MELA 0038)
Color was warm, because it was close to red. The pulse of light was uncomfortable. Thought of neon light. Part of the pulse was blurry at first, but they could then perceive the constancy of the pulse. Similar to first run. It seem a little more clear that first run. (MELA 0049)
Pulse felt more concentrated (meaning opaque) towards center, and almost blurry. Somewhat more blurry than previous pulses. (MELA 0050)
Rated smooth to jagged in regards to the onset/transition of the pulse from the background. The pulse is more comfortable to look at than the background. Was bright but not uncomfortable. Pulse was a lighter version of the background. (MELA 0073)
Pretty friendly. Seemed bright in intensity and character. Very illuminant. (MELA 0074)
Everything was kind of blurry, so it was difficult to make ratings. Pulses seemed the same the whole way through. More similar to LMS and Light Flux than to melanopsin. (MELA 0080)
Seemed like a light pink light that came on and off. Wintery: like the kind of light expected during a pretty winter's day. Kind of like light off of snow. Feels like all of the pulses are constant. (MELA 0082)
Pink and somewhat bright pulses. Kind of a dull orange, kind of colorless. (MELA 0088)
Pulses appeared neutral – seemed like a wall in a building - like a hospital or an office building. After the pulse goes away subject had trouble seeing until they blinked- might be that they were unable to focus, not totally sure. Fairly pretty, pleasant, neurtal-ish. Most of the properties, hue and brightness and aversiveness were very neutral. Like vanilla. (MELA 0094)
Pulse looked white, so rating colorless to colored was weird. Smooth to jagged was hard to rate. Pulse looked white again, colorless. For colorless to colored the rating reflected the change from the background. (MELA 0096)

Table S3. Pre-registrations and protocol deviations. Links are to pre-registration pages on the Open Science Framework site. Some pre-registrations include addenda.

URL	Experiment name and protocol deviations
https://osf.io/yzwm6	**fMRI Experiment 1, 400% Mel pulses** – Pulse-oximetry regressors were not used due to an error in the date field of the timestamps of the physio files. We discovered this error during a code audit after completing the analyses presented here. While it would be possible correct for this error in data analysis, we elected to not re-process our data to include the physiologic regressors, as these explain minimal variance within occipital cortex. – A Fourier basis set instead of an FIR basis set was used to model the fMRI data, given the asynchronous timing of events relative to TRs – The V1 region of interest was set to 5–25° (as opposed to 5–30°) as we wished to have additional stringency in avoiding signals from beyond the boundary of the stimulated field (which could contain rod intrusion) – Preliminary analyses of the LGN region of interest showed poor quality signals, so this was not pursued further – We have not pursued detailed analyses of the extra-striate regions of interest
https://osf.io/vqady	**fMRI Experiment 2, 400% LMS pulses**. Deviations as described for Experiment 1, and – The double-gamma model was found to produce poor fits to the evoked responses. This approach was discarded in favor of estimation of the shape of the HRF in individual subjects, and the use of the neural-step function model. – A proposed analysis would have examined differences between the LMS and Mel stimuli in evoking responses within the cortical and subcortical somatosensory system. These analyses have not yet been pursued.
https://osf.io/ayvb5	**fMRI Experiment 3, Splatter CRF**. Deviations as described for Experiment 1.
https://osf.io/w86pu	**fMRI Experiment 4, Mel CRF**. Deviations as described for Experiment 1.
https://osf.io/w95da	**fMRI Experiment 5, LMS CRF**. Deviations as described for Experiment 1.
https://osf.io/pv3a4	**fMRI Experiment 6, Rod control**. While pulse oximetry data were collected, these were not used so that the analyses of these data matched the analyses performed for the other experiments.
https://osf.io/u8ggn	**Perceptual rating of Mel and LMS pulses** – A set of 5 pre- and 5 post-experiment, validation measurements of the stimulus spectra were made and averaged. A small subset of these measurements (3 out of 750) featured clearly abnormal spectra due (we suspect) to a transient failure of device control. We excluded these spectra from the average that was generated across the validations.

1. Ishihara S (1977) *Tests for Colour-Blindness*. (Kanehara Shuppen Company, Ltd., Tokyo).
2. Spitschan M, Datta R, Stern AM, Brainard DH, Aguirre GK (2016) Human visual cortex responses to rapid cone and melanopsin-directed flicker. *Journal of Neuroscience* 36(5):1471–1482.
3. Spitschan M, Aguirre GK, Brainard DH (2015) Selective stimulation of penumbral cones reveals perception in the shadow of retinal blood vessels. *PloS one* 10(4):e0124328.
4. Spitschan M, Jain S, Brainard DH, Aguirre GK (2014) Opponent melanopsin and S-cone signals in the human pupillary light response. *Proceedings of the National Academy of Sciences* 111(43):15568–15572.
5. CIE (2006) Fundamental Chromaticity Diagram with Physiological Axes – Part 1, (Commission Internationale de l'Eclairage), Technical Report 170-1.
6. Asano Y, Fairchild MD, Blondé L (2016) Individual colorimetric observer model. *PloS one* 11(2):e0145671.
7. Brainard DH (1996) Cone contrast and opponent modulation color spaces in *Human color vision*, eds. Kaiser PK, Boynton RM. (Optical Society of America, Washington, DC), pp. 563–579.
8. Aguirre GK, Mattar MG, Magis-Weinberg L (2011) de Bruijn cycles for neural decoding. *NeuroImage* 56(3):1293–1300.
9. Dale AM, Fischl B, Sereno MI (1999) Cortical surface-based analysis: I. Segmentation and surface reconstructionSegmentation and surface reconstruction. *NeuroImage* 9(2):179–194.
10. Fischl B, Sereno MI, Dale AM (1999) Cortical surface-based analysis: II: Inflation, flattening, and a surface-based coordinate system. *NeuroImage* 9(2):195–207.
11. Fischl B, Sereno MI, Tootell RB, Dale AM, , et al. (1999) High-resolution intersubject averaging and a coordinate system for the cortical surface. *Human Brain Mapping* 8(4):272–284.
12. Fischl B, Dale AM (2000) Measuring the thickness of the human cerebral cortex from magnetic resonance images. *Proceedings of the National Academy of Sciences* 97(20):11050–11055.
13. Ségonne F, et al. (2004) A hybrid approach to the skull stripping problem in mri. *NeuroImage* 22(3):1060–1075.
14. Fischl B, et al. (2004) Automatically parcellating the human cerebral cortex. *Cerebral Cortex* 14(1):11–22.
15. Fischl B, et al. (2002) Whole brain segmentation: automated labeling of neuroanatomical structures in the human brain. *Neuron* 33(3):341–355.
16. Sled JG, Zijdenbos AP, Evans AC (1998) A nonparametric method for automatic correction of intensity nonuniformity in MRI data. *IEEE Transactions on Medical Imaging* 17(1):87–97.
17. Dale AM, Sereno MI (1993) Improved localization of cortical activity by combining EEG and MEG with MRI cortical surface reconstruction: a linear approach. *Journal of Cognitive Neuroscience* 5(2):162–176.
18. Fischl B, Liu A, Dale AM (2001) Automated manifold surgery: constructing geometrically accurate and topologically correct models of the human cerebral cortex. *IEEE Transactions on Medical Imaging* 20(1):70–80.
19. Ségonne F, Pacheco J, Fischl B (2007) Geometrically accurate topology-correction of cortical surfaces using nonseparating loops. *IEEE Transactions on Medical Imaging* 26(4):518–529.
20. Jo HJ, et al. (2013) Effective preprocessing procedures virtually eliminate distance-dependent motion artifacts in resting state fMRI. *Journal of Applied Mathematics* 2013.
21. Friston KJ, Williams S, Howard R, Frackowiak RS, Turner R (1996) Movement-related effects in fMRI time-series. *Magnetic Resonance in Medicine* 35(3):346–355.
22. Benson NC, Butt OH, Brainard DH, Aguirre GK (2014) Correction of distortion in flattened representations of the cortical surface allows prediction of V1-V3 functional organization from anatomy. *PLoS Computational Biology* 10(3):e1003538.
23. Aguirre GK, Zarahn E, D'Esposito M (1998) The variability of human, BOLD hemodynamic responses. *NeuroImage* 8(4):360–369.
24. CIE (1932) *Commission Internationale de l'Eclairage Proceedings*. (Cambridge University Press, Cambridge, UK).
25. Horiguchi H, Nakadomari S, Misaki M, Wandell BA (2009) Two temporal channels in human V1 identified using fmri. *NeuroImage* 47(1):273–280.
26. Adelson EH (1982) Saturation and adaptation in the rod system. *Vision research* 22(10):1299–1312.
27. Aguilar M, Stiles WS (1954) Saturation of the rod mechanism of the retina at high levels of stimulation. *Journal of Modern Optics* 1(1):59–65.
28. Hung SM, et al. (2017) Cerebral neural correlates of differential melanopic photic stimulation in humans. *NeuroImage* 146:763–769.
29. Tse PU, Baumgartner FJ, Greenlee MW (2010) Event-related functional MRI of cortical activity evoked by microsaccades, small visually-guided saccades, and eyeblinks in human visual cortex. *NeuroImage* 49(1):805–16.